Electrical, Optical, and Scanning Tunneling Microscopic Studies on Layer Type $CdIn_2S_{4-x}Se_x$ ($1.75 \leq x \leq 2.75$)

S. K. Srivastava, M. Pramanik, and D. Palit†

Department of Chemistry, Indian Institute of Technology, Kharagpur-721302, India

B. K. Mathur, A. K. Kar, and B. K. Samanta Ray

Department of Physics, Indian Institute of Technology, Kharagpur-721302, India

H. Haeuseler* and W. Cordes

Anorganische Chemie, Universität Siegen, D-57068 Siegen, Germany

Received March 14, 2001. Revised Manuscript Received July 20, 2001

The present paper deals with the microstructural parameters calculated from X-ray diffraction data, electrical and optical investigations, and scanning tunneling microscopy (STM) studies on $ZnIn_2S_4$ IIIa layer type $CdIn_2S_{4-x}Se_x$ ($1.75 \leq x \leq 2.75$) quaternary chalcogenides. Microstructural parameters such as dislocation density, root-mean-square strain, stacking fault probability, crystallite size anisotropy, and layer disorder parameters of these compounds have been calculated. The temperature variation of electrical conductivity (25−400 °C) confirmed semiconducting behavior. The band gaps of all these compounds obtained from STM and optical measurements are in the range 1.57−1.77 eV and are comparable to each other irrespective of the technique used.

Introduction

Ternary chalcogenides, AB_2X_4 (A = Al, Ga; B = Zn, Cd, and Hg; X = S, Se) have attracted much attention in recent years [see refs 1 and 2 and literature cited therein]. These compounds crystallize in three different types of structure: namely, spinel type for most of the indium compounds, thiogallate type for most of the gallium compounds, and a layer type $ZnIn_2S_4$ structure, for which different polytypes have been reported.[3] The common features of all these structure types are that (i) the anions form closed-packed arrays and (ii) the cations occupy tetrahedral and octahedral sites within these arrays. The difference is mainly due to the ratio between the number of octahedrally coordinated cations n_o to the number of tetrahedrally coordinated cations n_t. With respect to cation coordination the $ZnIn_2S_4$ structure ($n_o/n_t = 1:2$) is between the spinel ($n_o/n_t = 2:1$) and the thiogallate ($n_o/n_t = 0:3$) type structures. Synthesis of quaternary layered crystals by partial substitution of some of the atomic species has been reported. According to Razzetti and Lottici,[4] $ZnIn_2S_4$ layered phases should be obtained in sulfide systems with one end member crystallizing in the spinel structure and the other one in the thiogallate structure type. This concept, which is based on the site preference of the metal ions, has been improved by Lutz et al.[5] In some cases, new compounds crystallizing with $ZnIn_2S_4$ (IIIa) (Figure 1)[6] type structures were obtained either at a fixed composition, $CoGa_{1.5}Cr_{0.5}S_4$[7] $CoTi_{0.3}Ga_{1.7}S_4$,[8] or $MnTi_{0.4}Ga_{1.6}S_4$,[9] or for a limited range of homogeneity for, e.g., in the systems $CdIn_2S_4$ –$CdIn_2Se_4$,[10] $MnIn_2S_4$ –$MnIn_2Se_4$,[11] or $FeIn_2S_4$ –$FeIn_2Se_4$ [12] as a single phase. These layered materials are essentially interesting because of their anisotropic physical properties and find applications in the development of photodetectors, switches, and photovoltaic devices.[13] Recent investigations have also shown that lithium can be intercalated chemically[14] as well as electrochemically[15] for making these materials potential applicants in the development of primary and secondary batteries.

It should be noted that, among the different properties of these types of compounds, physical properties are largely influenced by the atomic arrangements in them as well as by the nature and extent of the defects present in their atomic arrangements. Prominent among these defects are strain, dislocations, and layer disorder

* Corresponding author. E-mail: sunit@chem.iitkgp.ernet.in.
† Present address: Department of Chemistry, University of Chittagong, Bangladesh.

(1) Hulliger, F. *Structural Chemistry of Layer Type Phases*; D. Reidel Publ.: Dordrecht, 1976; Vol. 5.
(2) Haeuseler, H.; Srivastava, S. K. *Z. Kristallogr.* **2000**, *215*, 205.
(3) Haeuseler, H. *J. Solid State Chem.* **1990**, *86*, 275.
(4) Razzetti, C.; Lottici, P. P. *Mater. Chem. Phys.* **1984**, *11*, 65.
(5) Lutz, H. D.; Buchmeier, W.; Siwert, H. *Z. Anorg. Allg. Chem.* **1996**, *533*, 118.
(6) Berand, N.; Range, K. J. *J. Alloys Compd.* **1994**, *205*, 295.
(7) Haeuseler, H.; Kwarteng-Acheampong, W. *Mater. Res. Bull.* **1989**, *24*, 939.
(8) Haeuseler, H.; Cordes, W. *Mater. Res. Bull.* **1990**, *25*, 1371.
(9) Haeuseler, H.; Cordes, W. *Mater. Res. Bull.* **1992**, *27*, 1057.
(10) Haeuseler, H. *J. Solid State Chem.* **1979**, *29*, 121.
(11) Schmidt, Ch.; Haeuseler, H. *Mater. Res. Bull.* **1995**, *30*, 585.
(12) Reil, S.; Haeuseler, H. *J. Alloys Compd.* **1998**, *270*, 83.
(13) Gentile, A. L. *Prog. Cryst. Growth Charact.* **1985**, *10*, 242.
(14) Ochel, M. Diploma Thesis, Universität Siegen, 1994.
(15) Bicelli Peraldo, L.; Maffi S.; Tagliavini, P.; Zanotti, L. *Solid State Ionics* **1987**, *24*, 297.

10.1021/cm0110829 CCC: $20.00
Published on Web 10/13/2001

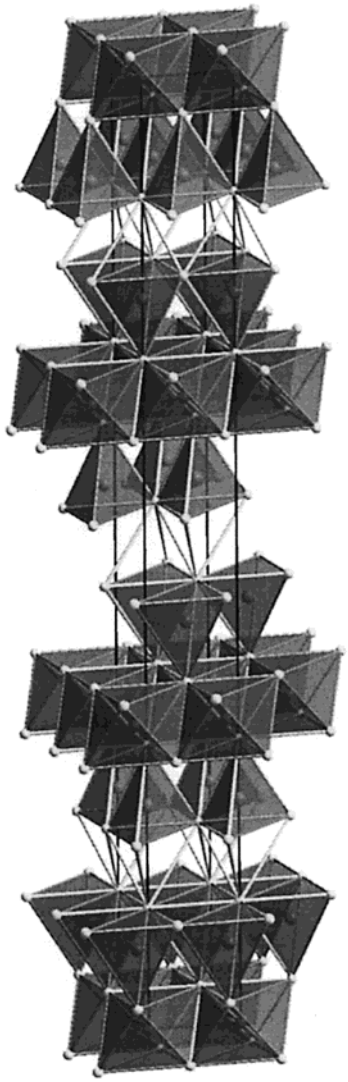

Figure 1. Layer type $ZnIn_2S_4$ (IIIa) structure of the $CdIn_2S_{4-x}Se_x$ compounds. The unit cell consists of three slabs built from two layers of tetrahedra connected to a central layer of octahedra. The slabs are separated by a van der Waals gap.

parameters. These are developed partly during growth of the crystallites and are due to the mechanical and thermal treatments to which the samples are subjected. The strength of materials is found to be dependent on size, lattice distortion, dislocations, stacking faults, etc. Hence, understanding the lattice defects and disorders in materials is of extreme importance in order to explain the electrical properties of these materials.

Scanning tunneling spectroscopy (STS), which probes the energy level spectrum, has been considered to be an effective method for understanding the electronic nature of surfaces.[16−18] Such measurements have been successfully employed to study a variety of surfaces, which include semiconducting surfaces,[19−22] delineated p−n junctions,[23] metal oxide semiconducting devices,[24] and superlattices.[25] It has been possible to obtain important information on band gaps, band edges, band bending, and superlattices. Topographic features along with the energy and spatial variation of the electronic density of states (DOS) are helpful to gain insight into the local surface nature of these layered chalcogenides in comparison to a few other reported layered materials.[17]

According to X-ray investigations in the systems $CdIn_2S_4$ –$CdIn_2Se_4$,[10] layered materials are formed for $CdIn_2S_{4-x}Se_x$ ($1.75 \leq x \leq 2.75$). In the literature, information on physical properties of these compounds is given only for the composition $CdIn_2S_2Se_2$.[26,27] The present paper highlights preparation of disordered $ZnIn_2S_4$ IIIa layer type $CdIn_2S_{4-x}Se_x$ ($1.75 \leq x \leq 2.75$) compounds and their characterization by X-ray diffraction, as well as electrical and optical properties. STS measurements are also carried out to understand the structures of DOS near the Fermi level and to estimate the band gaps at room temperature. These findings have been compared to those obtained from optical spectra. Surface features have also been studied using scanning tunneling microscopy (STM).

Experimental Section

In the present investigations, all the $CdIn_2S_{4-x}Se_x$ ($1.75 \leq x \leq 2.75$) compounds were prepared from the binary chalcogenides as reported by Haeuseler.[27] Appropriate amounts of the binary compounds, i.e., CdS, CdSe, In_2S_3, and In_2Se_3, were taken, and the reaction was carried out at 900 °C for a period of 4 days followed by a subsequent second and third heat treatment (which is needed to be sure that the reaction reached equilibrium) at 800 °C for 3 days each. After the third firing the samples were cooled slowly to room temperature.

X-ray diffractograms of all the samples were measured on a Philips 1729 diffractometer using monochromatic Cu Kα radiation. For this purpose samples were ground at room temperature and passed through a 200 mesh sieve. However, it has to be noted that by grinding of the samples one introduces additional strain and lattice imperfections in the crystallites. For this reason all the sample powders were annealed in evacuated ampules at 800 °C for 24 h. Accurate lattice parameters were obtained by a least-squares method.

Assuming that the broadening of the X-ray reflection is due to the presence of size broadening, strain broadening, and broadening arising from the variation of interlayer spacing, the intensity profiles of the 009 reflection in the X-ray diffractograms of all the samples were recorded. From these the microstructural parameters apparent crystallite size P_V and root-mean-square (rms) strain $\langle e^2 \rangle^{1/2}$ were calculated by adopting a single line technique similar to that described by

(16) Güntherodt, H. J.; Wiesendanger, R. *Scanning Tunneling Microscopy I: General principles and applications to clean and adsorbate-covered surfaces*; Springer-Verlag: Berlin, 1994.
(17) Wiesendanger, R. *Scanning Probe Microscopy and Spectroscopy: Methods and Applications*; Cambridge University Press: New York, 1994.
(18) Kasiviswanathan, S.; Srinivas, V.; Kar, A. K.; Mathurand, B. K.; Chopra, K. L. *Appl. Surf. Sci.* **1997**, *115*, 399.
(19) Srinivas, V.; Kasiviswanathan, S.; Barua, P.; Mathur, B.K. *Appl. Surf. Sci.* **1999**, *147*, 140.
(20) Kar, A. K.; Dhar, A.; Ray, S. K.; Mathur, B. K.; Bhattacharya, D.; Chopra, K. L. *Mater. Sci. Eng.* **1999**, *B68*, 10.
(21) Albrektsen O.; Arent, D. J.; Meier, H. P.; Salemink, H. W. M. *Appl. Phys. Lett.* **1990**, *57*, 31.
(22) Gwo, S.; Smith, A. R.; Shih, C. K.; Sadra, K.; Streetman, B. G. *Appl. Phys. Lett.* **1992**, *61*, 31.
(23) Yu, E. T.; Barmak, K.; Ronsheim, P.; Johnson, M. B.; McFarland, P.; Halbout, J. M.; Powell, A. R.; Iyer, S. S. *J. Appl. Phys.* **1996**, *79*, 2115.
(24) . Yu, E. I.; Halbout, J. M.; Powell, A. R.; Iyer, S. S. *Appl. Phys. Lett.* **1992**, *61*, 3166.
(25) Krishnan, K. M.; Modak, A. R.; Lukas, C. A.; Michel, R.; Cherry, H. B. *J. Appl. Phys.* **1996**, *79*, 5169.
(26) Tarricone, L.; Lottici, P. P. In *Ternary and Multinary Compounds*; Proc. 7th Int. Conf.; Deb, S. K., Zunger, A., Eds.; Materials Research Society: Pittsburgh, 1986.
(27) Paracchini, C.; Parisini, A.; Tarricone, L. *J. Solid State Chem.* **1986**, *65*, 40.

Mitra and Bhattacherjee.[28] Geometrical and background corrections were applied to the measured data as described by Mitra and Bhattacherjee.[29] The intensities were also corrected for Lorenz and polarization effects.[30] The true crystallite size P_F was determined by the method of Fourier analysis. The magnitudes of mean fractional change in the interlayer distance g in the direction of d_{009} and the fraction γ of planes affected by layer disorder have been calculated according to the techniques described by Wilson[31] and Mitra.[32]

The dislocation density ρ has been calculated according to Williamson and Smallman,[33] and the stacking fault probability α, i.e., the fraction of layers undergoing stacking sequence faults in a given crystal, has been calculated according to Warren.[34]

Electrical conductivity measurements were performed using a two-probe method on compressed, sintered pellets in the temperature range 25−400 °C in an inert atmosphere. The optical spectra were recorded on a Shimadzu UV−vis spectrophotometer.

STM studies were made on all these compounds in the form of compressed pellets by using a commercial STM (RKH Technology Inc., USA). The tunneling spectra were acquired by freezing the tip in a position corresponding to a tunneling current of 300 pA and different tip-to-sample voltages. Each voltage corresponds to a particular tip-to-sample distance. The current−voltage ($I-V$) data were acquired with the feedback loop interrupted by the sample and hold circuit.[17,18] The signals were averaged to over 10 spectra at each sample. Reproducibility was checked by acquiring data at different locations and at different tip-to-sample distances using tungsten and mechanically cut platinum−iridium tips. The dynamic conductance (dI/dV) and the normalized dynamic conductance [$(dI/dV)/(I/V)$] were recorded by taking the numerical derivative of the $I-V$ data. These normalized [$(dI/dV)/(I/V)$] curves represent a normalized density of states (DOS).

Results and Discussion

All investigated compounds $CdIn_2S_{4-x}Se_x$ ($1.75 \leq x \leq 2.75$) are reddish brown in color. According to the X-ray diffractograms all samples are single phase.[10,35] The variation of the lattice parameters a and c with composition shows that both a and c increase with increasing selenium content in $CdIn_2S_{4-x}Se_x$. These values are in good agreement with a $ZnIn_2S_4$ (IIIa) type structure with space group $R3m$ as reported by Cordes.[35] In each specimen, the 009 reflection is of maximum intensity, indicating thereby a strong orientation along the c-axis. However, the other 00l reflections are of relatively weaker intensity. The intensities for 10l reflections gradually increase with increasing selenium contents in the samples, attain a maximum for $CdIn_2Se_{2.50}S_{1.50}$, and then fall gently. However, 11l reflections in general do not show any definite trend with respect to intensity variation. It is noted that the 116 and the 119 reflections showed opposite variation in intensity. The observed changes in the intensities and especially the broadening of some reflections indicate that the substitution of sulfur in these compounds has definitely introduced some layer disorder.

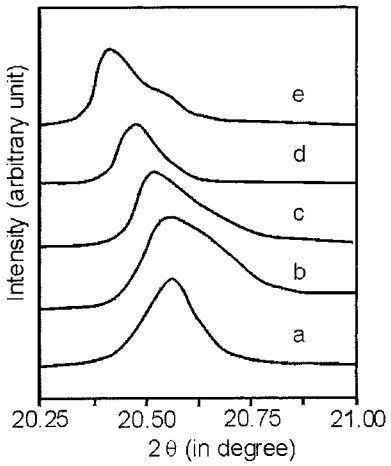

Figure 2. X-ray diffraction profiles for 009 reflection of (a) $CdIn_2S_{2.25}Se_{1.75}$, (b) $CdIn_2S_2Se_2$, (c) $CdIn_2S_{1.75}Se_{2.25}$, (d) $CdIn_2S_{1.50}Se_{2.50}$, and (e) $CdIn_2S_{1.25}Se_{2.75}$.

The X-ray diffraction profiles for the 009 reflection of the different $CdIn_2S_{4-x}Se_x$ ($1.75 \leq x \leq 2.75$) compounds used for the calculation of microstructural parameters are displayed in Figure 2. A gradual shift of the peak maximum as well as broadening of the peak is observed from sample a to sample e. Furthermore, it is also noted that the peaks are asymmetric as they rise more steeply on the low-angle side than on the high-angle side. It is well-known that such asymmetric behavior is due to the presence of layer disorder.

The crystallite sizes P_V and P_F obtained by the method of variance and the Fourier analysis, respectively, rms strain $\langle e^2 \rangle^{1/2}$, dislocation density ($\rho$), fractional change ($g$) in interlayer spacing, the fraction (γ) of the planes affected by defects, stacking fault probability (α), and crystallite size anisotropy (P_{009}/P_{101}) for $CdIn_2S_{4-x}Se_x$ ($1.75 \leq x \leq 2.75$) are presented in Table 1. It is noted that for all compositions the crystallite sizes obtained by the variance method are lower than that calculated by the Fourier method. This is expected because, unlike the variance technique, the size of the crystallites determined by the Fourier technique is not influenced by the defect broadening.

From all these data it can be seen that the predominant composition is that with $x = 2$ as for the crystallites of $CdIn_2S_2Se_2$ the highest crystal size is obtained, combined with the smallest rms strain, the smallest dislocation density ρ, and smallest values for the fraction of planes being affected by defects γ, but the highest values for the stacking fault probability α and crystal size anisotropy P_{009}/P_{101}. Similarly for the compound for which the second highest crystal size is obtained, $CdIn_2S_{1.25}Se_{2.75}$, the microstructural parameters rms strain, dislocation density, and the fraction of planes being affected by defects γ exhibit the second lowest values while the stacking fault probability α and the crystal size anisotropy P_{009}/P_{101} have the second highest values. This clearly indicates that for these compositions special situations are reached that may be due to some type of ordering of the two different anions, the cations, or both. Microstructural pictures for such ordering schemes taking into account these observations have yet to be developed.

Table 1 also shows that both the stacking fault probability (α) and the crystallite size anisotropy (P_{009}/

(28) Mitra, G. B; Bhattachaerjee, S. *Am. Mineral.* **1969**, *54*, 1409.
(29) Mitra, G. B.; Bhattachaerjee, S. *Acta Crystallogr.* **1970**, *B26*, 2124.
(30) Stanjek, H.; Niederbudde, E. A.; Hausler, W. *Clay Miner.* **1992**, *27*, 3.
(31) Wilson, A. J. C. *X-ray Optics*; Mathuen: London, 1962.
(32) Mitra, G. B. *Z. Kristallogr.* **1963**, *119*, 161.
(33) Williamson, B.; Smallman, R. C. *Philos. Mag.* **1956**, *1*, 34.
(34) Warren, B. E. *X-ray Diffraction*; Addison-Wesley: Reading, MA, 1969.
(35) Cordes, W. Ph.D. Thesis, Universität Siegen, 1994.

Table 1. Microstructural and Layer Disorder Parameters of $CdIn_2S_{4-x}Se_x$ ($1.75 \leq x \leq 2.75$) Compounds

compound	crystallite size (Å) P_V	crystallite size (Å) P_F	$\langle e^2\rangle^{1/2}$ (10^{-3})	ρ (10^{15} lines/m^2)	g	g	P_{009}/P_{101}	a
$CdIn_2S_{2.25}Se_{1.75}$	230	235	3.00	1.10	0.050	0.004	1.13	0.08
$CdIn_2S_2Se_2$	290	340	0.84	0.19	0.020	0.001	2.29	0.55
$CdIn_2S_{1.75}Se_{2.25}$	110	120	1.70	1.30	0.005	0.006	1.09	0.11
$CdIn_2S_{1.50}Se_{2.50}$	150	225	5.00	1.50	0.036	0.011	1.18	0.12
$CdIn_2S_{1.25}Se_{2.75}$	265	290	1.10	0.32	0.010	0.002	1.67	0.34

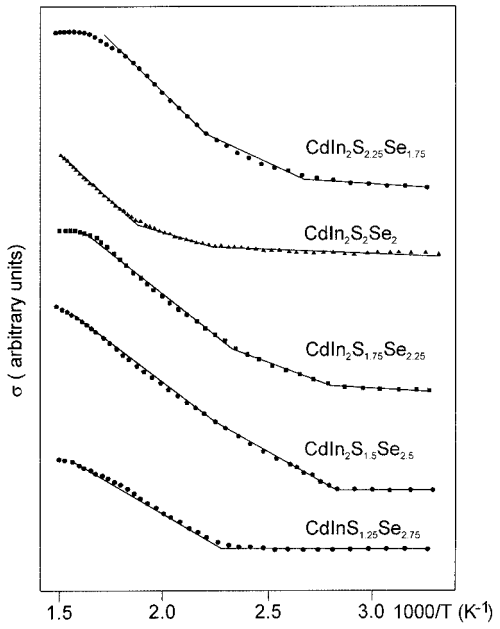

Figure 3. Electrical conductivity (σ) versus $1/T$ plots for $CdIn_2S_{4-x}Se_x$ compounds. The absolute values of the room temperature conductivities are given in Table 2. The conductivity at 400 °C is determined by the measuring system to $10^{-0.5}$ (Ω^{-1} cm^{-1}) in all cases.

P_{101}) vary in the same way with the crystallite size. Both parameters fall linearly with the crystal size down to $P_F = 235$ Å and remain nearly constant for smaller crystals. It is also observed that the variation of rms strain $\langle e^2\rangle^{1/2}$ is quite similar to that of the fractional change (g) in interlayer spacing and of the fractions of planes affected by disorder (γ), indicating thereby a relationship between these parameters. Thus the strain in the crystals can be minimized by a lower number of disordered planes. This on the other side leads to a larger anisotropy of the crystal growth as can be seen from the growing ratio P_{009}/P_{101}.

The temperature dependence (25−350 °C) of the electrical conductivity (σ) for the different samples of $CdIn_2S_{4-x}Se_x$ ($1.75 \leq x \leq 2.75$) is shown in Figure 3. These studies confirm a semiconducting behavior of these compounds. As can be seen from these plots, there exists a temperature range above room temperature for which the plots are linear with a very small (≈0.03 eV) activation energy for all samples. The small activation energy indicating the predominance of extrinsic (impurity) conduction process results may be from shallow donor levels due to some chalcogen atom vacancies.

Above about 270 °C the activation energy for all the compounds is ≈0.63 eV except for $CdIn_2S_{1.75}Se_{2.25}$, where it is relatively low (0.42 eV). There is no marked dependence of the activation energy on the composition. In this temperature region we assume intrinsic conduction resulting from the thermal activation across the energy gap. However, as these values are still much smaller than the values obtained from optical measurements, we think that the smallest energy gap is not a direct one.

Table 2. Band Gaps for $CdIn_2S_{4-x}Se_x$ ($1.75 \leq x \leq 2.75$) from Tunneling Spectra and Optical Measurements and Electrical Conductivities σ at Room Temperature

x	band gap in eV: tunneling spectra[a]	band gap in eV: optical method[b]	log σ/(Ω cm)
1.75	1.77	1.72	3.3
2.00	1.68	1.68	3.0
2.25	1.66	1.67	3.4
2.50	1.63	1.64	4.0
2.75	1.55	1.57	2.2

[a] See Figure 5. [b] See Figure 4.

Furthermore, it is interesting to note that in the cases of $CdIn_2S_2Se_2$ and $CdIn_2S_{2.25}Se_{1.75}$, i.e., those compounds with a high sulfur content, an intermediate temperature zone (115−200 °C) exists for which also the graph is linear but with an activation energy of 0.17−0.20 eV. There are a number of possible interpretations of this finding, such as (i) a temperature dependence of the charge carrier mobility (μ),[36−38] (ii) a variation of the potentials at the grain boundaries as shown by Werner,[39] and (iii) the existence of a second set of donor or acceptor levels deeper in the forbidden gap. Which of these possibilities applies in those cases needs further investigation.

The electrical conduction mechanism in polycrystalline semiconductors as mentioned in our earlier discussion is vastly influenced by the inherent intercrystalline boundaries. These grain boundary regions are dominated by a network of dislocations which are accompanied by large strain fields. Like grain boundaries, these dislocations also act as scattering centers for the charge carriers. The situation is quite complicated in compound semiconductors especially in highly anisotropic layered structures. Although accurate modeling is a very difficult task, several models[40,41] exist where, inside the crystallite, a series of distinct high conductivity (bulk) and low conductivity (grain boundary) regions are considered. Some of these models predict a dependence of the mobility on the crystallite size. Hence, small crystallites possess low mobility and lower conductivity as compared to larger crystallites. As can be seen from the room temperature conductivities (σ_{298K}) of different samples $CdIn_2S_{4-x}Se_x$ ($1.75 \leq x \leq 2.75$) (see Table 2 and Figure 3) and crystal sizes (see Table 1), there is no

(36) Andriyashik, M. V; Sakhnovskii, M. V; Timofev, Y. B.; Yakimova, A. S. *Phys. Status Solidi* **1968**, *28*, 277.
(37) Suzuki, H.; Mori, S. *J. Phys. Soc. Jpn.* **1984**, *19*, 1082.
(38) Endo, S.; Irie, T. *J. Phys. Chem. Solids* **1976**, *37*, 201.
(39) Werner, J. H. *Solid State Phenom.* **1994**, *213*, 37−38.
(40) Suzuki, H.; Mori, S. *J. Phys. Soc. Jpn.* **1984**, *19*, 1082.
(41) Endo, S.; Irie, T. *J. Phys. Chem. Solids* **1976**, *37*, 201.

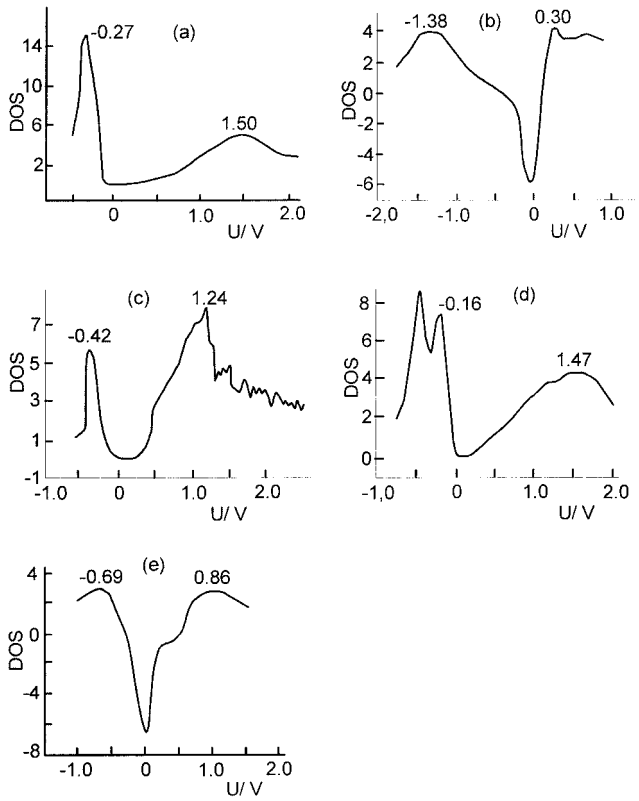

Figure 4. Plot of normalized DOS as a function of bias voltage U calculated from local tunneling spectra obtained from a scanning tunnel microscope for (a) $CdIn_2S_{2.25}Se_{1.75}$, (b) $CdIn_2S_2Se_2$, (c) $CdIn_2S_{1.75}Se_{2.25}$, (d) $CdIn_2S_{1.50}Se_{2.50}$, and (e) $CdIn_2S_{1.25}Se_{2.75}$.

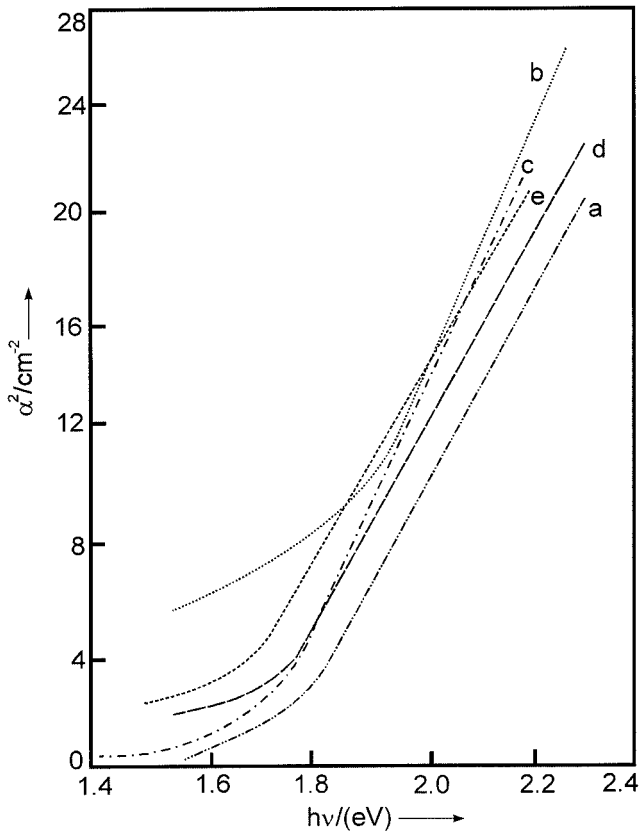

Figure 5. Plot of the absorption coefficient α^2 versus $h\nu$ for (a) $CdIn_2S_{2.25}Se_{1.75}$, (b) $CdIn_2S_2Se_2$, (c) $CdIn_2S_{1.75}Se_{2.25}$, (d) $CdIn_2S_{1.50}Se_{2.50}$, and (e) $CdIn_2S_{1.25}Se_{2.75}$.

significant correspondence between the size and the conductivity as suggested by these models. However, when the carrier concentration also changes for these compound semiconductors, the overall change in conductivity has to be attributed to both of these causes. Therefore, a linear dependence between size and conductivity cannot be expected as the generation of charge carriers is affected by the lattice defects which vary strongly within this group of samples.

Local tunneling spectroscopy (LTS) data were acquired by using the STM in spectroscopic mode at various locations on the surface of the samples with a constant tip−sample separation (s). By acquiring I vs V curves at various s values, we effectively measure the tunneling current over a wide range until we reach the limit of sensitivity, which is a few picoamperes. The $I-V$ curves recorded in this way are typical for semiconducting behavior and thus confirm the results of the conductivity measurements. The characteristics are reproducible, and essentially similar spectra could be obtained on different sites of the sample surface.

The band gaps of $CdIn_2S_{4-x}Se_x$ ($1.75 \leq x \leq 2.75$) compounds as obtained from the DOS plots (Figure 4) are compiled in Table 2. They decrease systematically with increasing selenium contents (x) in the compounds from 1.77 eV for $CdIn_2S_{2.25}Se_{1.75}$ to 1.55 eV for $CdIn_2S_{1.25}Se_{2.75}$.

The absorption coefficient (α) is related to the incident photon energy ($h\nu$) as[42]

$$\alpha = \beta(h\nu - E_g)^n$$

where E_g is the energy gap and $n = 1/2$ for a direct allowed transition and is independent of the transition probability. Figure 5 shows the plots of α^2 versus $h\nu$ for $CdIn_2S_{4-x}Se_x$ ($1.75 \leq x \leq 2.75$) compounds. The intercepts of the linear part of these plots on the energy axis at $\alpha = 0$ gives the band gaps of these compounds. These direct optical band energy values were found to be 1.72, 1.68, 1.67, 1.64, and 1.57 eV for $CdIn_2S_{2.25}Se_{1.75}$, $CdIn_2S_2Se_2$, $CdIn_2S_{1.75}Se_{2.25}$, $CdIn_2S_{1.50}Se_{2.50}$, and $CdIn_2S_{1.25}Se_{2.75}$, respectively.

Thus we observe that the values for the band gap energies obtained from the optical method and by scanning tunneling microscopy are nearly identical, although the tunneling microscopy yields band gap values slightly lower than those from optical data (Table 2).

Conclusions

X-ray diffraction studies of the phase $CdIn_2S_{4-x}Se_x$ confirmed that all compositions with ($1.75 \leq x \leq 2.75$) crystallize with the layered $ZnIn_2S_4$ IIIa type structure. The temperature dependence of the conductivity for all these compounds confirmed that they are semiconducting. The variation of the room temperature conductivity cannot be correlated with microstructural parameters of the compounds calculated by analysis of X-ray diffraction data, especially with the size of the crystallites. The variation of tunnel gap bias versus voltage spectra based on STM for all these compounds also shows typical semiconducting behavior. The band gap energies

(42) Pankove, J. I. *Optical processes in Semiconductors*; Prentice Hall Inc.: London, 1971.

deduced from optical spectra are nearly identical with that inferred from DOS plots obtained by STM.

Acknowledgment. We are grateful to the Council of Scientific and Industrial Research, HRDG, India, for financial support provided during this research. Thanks are also due to Mr. Subhashis Gangppadhyay for his help during the course of investigation.

CM0110829